RSC Advances

PAPER

View Article Online
View Journal | View Issue

Cite this: *RSC Adv.*, 2017, 7, 4269

Synthesis of well-dispersed ZnO–Co–C composite hollow microspheres as advanced anode materials for lithium ion batteries

Xiangjun Lu,* An Xie, Chunhai Jiang, Mi Lu, Yong Zhang, Haichang Zhong and Shuxin Zhuang

Received 15th November 2016
Accepted 20th December 2016

DOI: 10.1039/c6ra26816a

www.rsc.org/advances

In this study, ZnO–Co–C composite hollow microspheres made up of massive nanometer-sized subunits are fabricated through a facile adsorption treatment at room temperature, followed by heating processing in inert atmosphere. When they function as active materials in lithium ion batteries, the as-obtained ZnO–Co–C composites show good electrochemical properties in terms of relatively high first coulombic efficiency, high specific capacity, distinguished cyclic property and exceptional rate capacity. ZnO–Co–C composite hollow microspheres possess an initial coulombic efficiency of about 70.1%, which is one of the best results for ZnO-based anodes reported. During repetitive lithiation–delithiation 300 times, a high discharge capacity of 794 mA h g^{-1} is harvested at 200 mA g^{-1}. The unique advantages, including metal Co and carbon modification, hierarchical hollow architecture and the nanoscale building blocks, account for the superiority in electrochemical performance of the ZnO–Co–C composites.

1. Introduction

Rechargeable lithium ion batteries with higher specific capacity, longer cyclic lifespan and more notable rate capability are urgently needed for the rapid development of power grids, electric vehicles, hybrid electric vehicles, spaceflight and so on.[1–3] Nevertheless, the current graphite anode cannot satisfy the ever-growing demands of lithium ion batteries with high energy and power density due to its limited theoretical capacity (372 mA h g^{-1}) and inferior rate capability.[4] In addition, the safety issue caused by the lithium dendrites is another vital factor that needs to be conquered essentially. Nowadays, transition metal oxides utilized as potential electrode candidates in lithium ion batteries have received substantial interest by virtue of their higher theoretical capacity as well as moderate lithiation voltage that enables them to hamper the formation of lithium dendrites.[5–10] Among various transition metal oxides, zinc oxide (ZnO), apart from the merits of abundant resource, nontoxicity, morphological diversity and environmental benignity, holds bright prospects as an electrochemical active material on account of its relatively large theoretical capacity (978 mA h g^{-1}; almost three times that of the graphite anode) because of the conversion and alloying reaction mechanisms. Nonetheless, the large-scale application of ZnO electrodes is greatly prohibited by the massive capacity fading and inferior rate capability, respectively, caused by the severe structure deterioration (huge volume variation) and poor electronic conductivity. Moreover, the low initial coulombic efficiency of ZnO electrodes, which is common for almost all metal oxide electrodes, is another issue that needs to be ameliorated.

It is well established that devising metal oxide electrode materials as hollow structures is an effective avenue to improve their cycling stability.[11–15] The interior void space of hollow micro-nanostructures can relieve the large mechanical stress resulting from the drastic volume expansion–contraction during repetitive lithiation/delithiation by supplying an extra accommodating space, which is conducive to maintain the structural integrity, restrict the pulverization of the electrode and thus prolong the cyclic lifespan. For instance, Lou's group synthesized hierarchical Fe_3O_4 hollow and solid spheres *via* a facile solvothermal route, followed by annealing treatment.[15] When adopted as the electrochemical active materials in lithium ion batteries, the fabricated Fe_3O_4 hollow spheres revealed higher reversible capacity and more excellent cyclability than solid ones. It was claimed that the hollow construction of the Fe_3O_4 spheres plays a crucial role in obtaining enhanced electrochemical performance. Metals or carbonaceous materials are usually good conductors of electrons and the electronic conductivity of metal oxide electrodes can be enhanced to some extent when coupled with other metal oxides due to their synergetic effect. For example, a ternary $NiCo_2O_4$ electrode demonstrates enhanced electronic conductivity and electrochemical activity in comparison with binary nickel oxide and cobalt oxide.[16] Thus, with respect to poor electronic conductivity, modifying the metal oxides' active

---

Key Laboratory of Functional Materials and Applications of Fujian Province, School of Material Science and Engineering, Xiamen University of Technology, Xiamen 361024, P. R. China. E-mail: luxiangjun0531@163.com; Fax: +86 0592 6291326; Tel: +86 0592 6291323

materials with metals, carbonaceous materials and other metal oxides has been confirmed to be a useful strategy.[17–25] Furthermore, a few metal particles, such as Co, Fe and Ni nanoparticles, also demonstrate the catalytic effect to activate or accelerate the reversible decomposition of some SEI components, being propitious to the improvement of specific capacity and electrochemical reaction reversibility.[26–29]

In the past decade, considerable efforts have been paid to elevate the lithium storage performance of ZnO anodes through the aforementioned diverse strategies.[30–35] To date, although great progress has been achieved, the commercial application of ZnO anodes is still extremely challenging and the lithium storage properties need further improvement, particularly in cyclability and the initial coulombic efficiency. In this study, ZnO–Co–C composite hollow microspheres made up of numerous homogeneous ZnO and Co nanoparticles as well as the three dimensional carbon network throughout the entire hollow microsphere, have been synthesized *via* a simple two-step approach. To the best of our knowledge, the successful synthesis and the electrochemical performance of well-dispersed ZnO–Co–C composite hollow microspheres has not been reported so far. When working as the active materials in lithium ion batteries, the acquired hybrids manifest outstanding battery performance in terms of relative high reversible capacity, long cyclic lifespan, eminent rate performance and decent initial coulombic efficiency. The reasons for the superior electrochemical properties of ZnO–Co–C composites are interpreted in detail.

2. Experimental

2.1 Synthesis of precursor and ZnO–Co–C composites

Zinc citrate solid microspheres with rough surfaces were produced first of all according to a modified route reported in the previous literature.[36] In a typical synthetic procedure, the newly harvested zinc citrate solid microspheres with rough surfaces (0.1 g) were uniformly dispersed into 30 mL of cobalt nitrate solution with a concentration of 0.05 M under the assistance of ultrasonic processing for 15 min. The resulting suspension was aged at room temperature for 60 min, and then the precipitate (zinc–cobalt citrate precursor, 0.073 g) could be collected after filtration, rinsed with distilled water and dried at 60 °C for more than 12 h. By annealing the obtained precursor at 500 °C for 2 h in Ar, the corresponding ZnO–Co–C composites (0.052 g) were successfully synthesized and the final yield of ZnO–Co–C composites was about 52.0% on the basis of the initial zinc citrate solid microspheres. For comparison, the ZnO–C microspheres were prepared by calcination of zinc citrate solid microspheres in an Ar atmosphere without aging treatment in cobalt nitrate solutions.

2.2 Characterizations of precursor and ZnO–Co–C composites

X-ray diffraction (Bruker D8 X-ray diffractometer, Cu-K$_\alpha$ radiation 40 kV) was used to identify the phase of the obtained products. Scanning electron microscopy (SEM) and transmission electron microscopy (TEM) were carried out on ZEISS SIGMA and JEM-2100 instruments, in order to evaluate the morphology and microstructures of the products. The TriStar 3020 system was employed to characterize the specific surface area and pore diameter distribution of the collected product. The Raman spectroscopy and thermogravimetric (TG) analysis were carried out on LabRAM HR and STA 449 F3 Jupiter instruments, respectively. The inductively coupled plasma (ICP) measurement was performed on an ICP mass spectrometer (ICP-MS-4500).

2.3 Electrochemical evaluations

Coin-type 2025 cells were produced in an Ar-filled glove box, with water and oxygen content below 1.0 ppm, using a metallic lithium disk as the counter electrode. 1 M LiPF$_6$ in equal volumes of ethylene carbonate (EC) and diethyl carbonate (DEC) and Celgard 2350 acted as the electrolyte and separator, respectively. A uniform slurry made up of 70 wt% of the obtained ZnO–Co–C samples, 20 wt% of acetylene black and 10 wt% of poly(vinyl difluoride) (PVDF) was prepared under vigorous stirring and coated on a copper foil together with the finally drying process at 80 °C overnight in vacuum to produce the working electrode. The mass loading density of active materials is about 0.9–1.0 mg cm^{-2}. The electrochemical properties in terms of reversible capacity, cyclability and rate capability were tested on a battery electrochemical test system (LAND), and cyclic voltammetry investigations were undertaken on a CHI 604E electrochemical workstation.

3. Results and discussion

The morphology and microstructures of the pre-prepared zinc citrate solid microspheres were assessed *via* SEM and TEM techniques. The panoramic SEM micrograph shown in Fig. 1a hints that the solid microspheres have an average diameter of approximately 1.7 μm and disperse well. The high amplification SEM image (Fig. 1b) shows an individual zinc citrate microsphere and the zinc citrate on the surface of solid microsphere is apparent, which is further certified by TEM measurement illustrated in Fig. 1c. During the aging treatment in a solution containing Co^{2+}, the pre-prepared zinc citrate solid microspheres with rough surfaces would interact with Co^{2+} by means of the electrostatic interactions between the negative carboxylate acid groups (–COO$^-$) in zinc citrate and the positive Co^{2+} ions in the solution, resulting in the absorption of Co^{2+} ions on the rough surfaces of the zinc citrate solid microspheres, further resulting in the generation of the zinc–cobalt citrate shells. After that, the inner zinc citrate in the solid microspheres would dissolve gradually with increasing aging time and partially redeposit on the outer zinc–cobalt citrate shells (Ostwald ripening process), resulting in the increase of shell thickness and final formation of zinc–cobalt citrate hollow microspheres.[37] The SEM and TEM micrographs of the obtained precursor are displayed in Fig. 2. Distinctly, zinc–cobalt citrate microspheres show the rough and loose surfaces, which is quite different to the initial zinc citrate solid microspheres (Fig. 2a

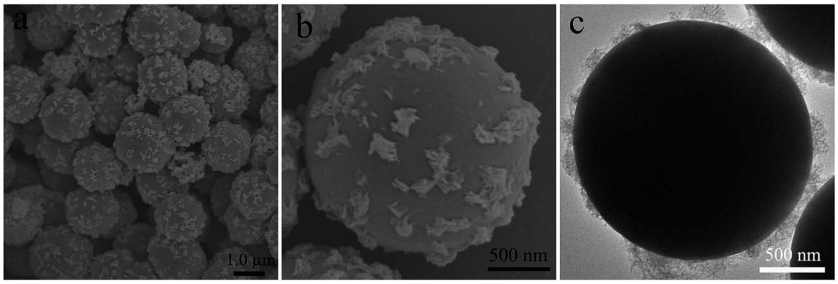

Fig. 1 The (a and b) SEM and (c) TEM micrographs of zinc citrate solid microspheres with rough surfaces.

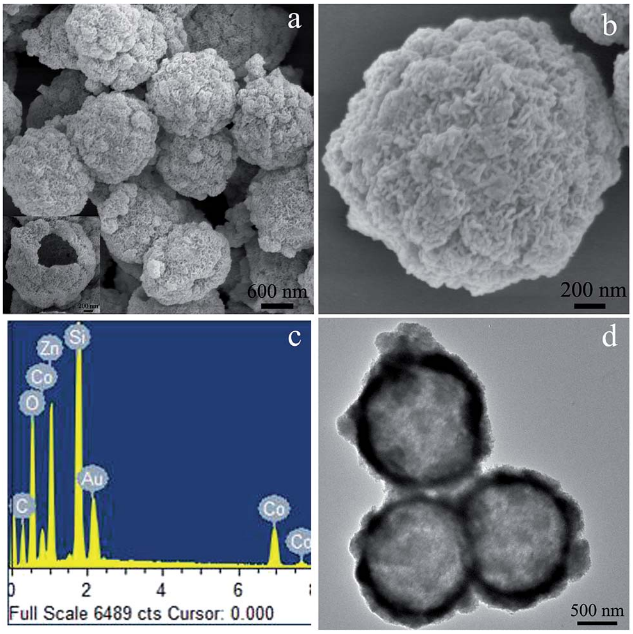

Fig. 2 The (a and b) SEM, (c) EDS pattern and (d) TEM micrographs of the collected zinc–cobalt citrate precursor.

and b). A cracked microsphere revealed in the inset of Fig. 2a displays the inner void space of zinc–cobalt citrate microsphere, and the average thickness of the shell is about 250 nm. EDS investigation (Fig. 2c) suggests that the precursor consists of Zn, Co and O elements, implying the absorption of Co^{2+} on zinc citrate microspheres. The signals of Si and Au are derived from the Si substrate and the coated conductive Au layer used for SEM examination, respectively. The TEM image represented in Fig. 2d further confirms the hollow architecture of the harvested precursor microspheres, coinciding well with the above-mentioned SEM observation (the inset in Fig. 2a). The XRD pattern (Fig. 3a) of zinc–cobalt citrate microspheres indicates the main amorphous feature of the precursor, which is analogous to the literature result.[36] Consequently, it can be claimed that zinc–cobalt citrate hollow microspheres are fabricated *via* a facile aging process.

By calcination of precursor microspheres at 500 °C for 2 h in Ar, ZnO–Co–C composites can be produced. The diffraction peaks originating from hexagonal ZnO (JCPDS card no. 36-1451) and cubic Co metal (JCPDS card no. 15-0806) can be found clearly from the XRD pattern illustrated in Fig. 3a. The absorbed Co^{2+} ions on the zinc–cobalt citrate precursor convert to metallic Co nanoparticles that disperse homogeneously throughout the entire microsphere during the heating process in the inert atmosphere. The carboxylate acid groups ($-COO^-$) in the precursor would carbonize *in situ* to form the three dimensional carbon network throughout the entire microsphere. Nonetheless, the absence of carbon diffraction peaks indicates the amorphous characteristic of the derived carbon. The broadening diffraction peaks of ZnO and Co are due to the three-dimensional carbon network that is capable of suppressing the growth and agglomeration of ZnO and Co nanoparticles during heat treatment, leading to the small crystallite sizes. The crystal size of ZnO is calculated to be 19.1 nm according to the Scherrer equation, being in line with the SEM result (Fig. 4c). The Raman spectra of ZnO–Co–C and ZnO–C composites are depicted in Fig. 3b. Two strong peaks centered at about 1360 and 1598 cm^{-1} can be seen clearly for both samples and attributed to the D and G bands of carbon, respectively, distinctly indicating the presence of carbon.[38] It has been well established that the decoration of metallic Co is capable of enhancing the graphitization degree of carbon, accounting for the stronger intensity of the G band for ZnO–Co–C composites in comparison with ZnO–C counterparts.[39] The enhancement of the graphitization degree of carbon is good for the improvement of electronic conductivity of active particles and thus the electrochemical performance.

Illustrated in Fig. 4a and b are the low magnification SEM micrographs of ZnO–Co–C composites, from which one can explicitly observe that the hybrids show an average diameter of 1.1 μm, which shrinks slightly in comparison with the zinc–cobalt citrate precursor. Fig. 4c shows an individual microsphere that is composed of a great deal of ZnO and Co nanoparticles, which contact intimately with each other. The TG curve of ZnO–Co–C composite microspheres is shown in Fig. 3c, from which two-step weight losses can be seen clearly. The weight loss below 200 °C is due to the evaporation of the absorbed moisture in the composites and the one between 250–450 °C is ascribed to the combination of the oxidation of metallic Co and the combustion of carbon. In an effort to determine the accurate contents of various components in the hollow composites, ICP measurement was performed. The results indicate that the accurate contents of ZnO, Co and C in composites are calculated to be about 75.1%, 8.5% and 16.4%,

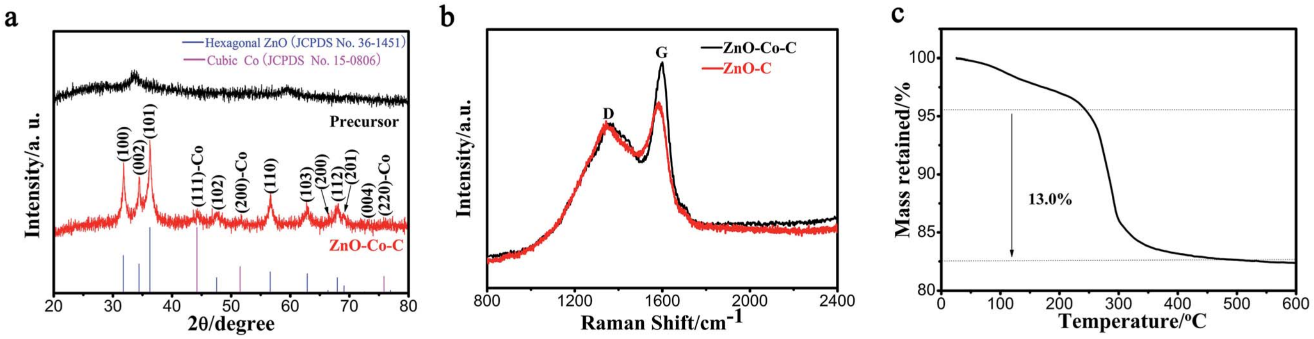

Fig. 3 (a) The XRD patterns of the collected zinc–cobalt citrate precursor and ZnO–Co–C composites. (b) The Raman spectra of ZnO–Co–C and ZnO–C composites. (c) TG curve of ZnO–Co–C composites.

respectively. The TEM images (Fig. 4d and e) evidence the hollow configuration of ZnO–Co–C composites, indicating that a good morphology is retained during the heating process. As shown in Fig. 4f, the HRTEM image collected from the white circle area in Fig. 4e reveals two sets of lattice fringes with the interplanar spacing of 0.271 nm and 0.205 nm, ascribed to the (100) plane of hexagonal ZnO and the (111) plane of cubic Co, respectively. The SAED pattern (inset in Fig. 4f) suggests the simultaneous presence of ZnO and Co, along with the polycrystalline characteristic of the composite hollow microspheres. The HAADF scanning TEM (STEM) micrograph and the element mappings of ZnO–Co–C composite hollow microspheres are depicted in Fig. 4g and h, respectively, wherein Zn, Co, O and C elements distribute homogeneously within the entire microsphere, further evidencing the well-dispersed ZnO and Co nanoparticles and the successful synthesis of ZnO–Co–C composites with good component distribution. It has been certified that the specific surface area of active particles is an important factor that exerts notable effects on their electrochemical performance. Thereby, the specific surface area and the pore diameter distribution of ZnO–Co–C composite hollow microspheres are tested by N_2 adsorption–desorption measurements at 77 K. As illustrated in Fig. 5a, ZnO–Co–C composite hollow microspheres represent the typical type IV isotherm profile, indicative of the mesoporous structures. The BET surface area is determined to be 80.0 $m^2\ g^{-1}$. The relatively large specific surface area of active particles can enlarge the contact area between the electrode and electrolyte, benefiting the improvement of reversible capacity and the reduction of electrode polarization.[40,41] The pore size distribution (Fig. 5b) originated from the Barrett–Joyner–Halenda approach suggests that the mesopores of composite microspheres mainly center around 6.4 nm, which is induced by the release of gas resulting from the decomposition of organic groups in zinc–cobalt citrate

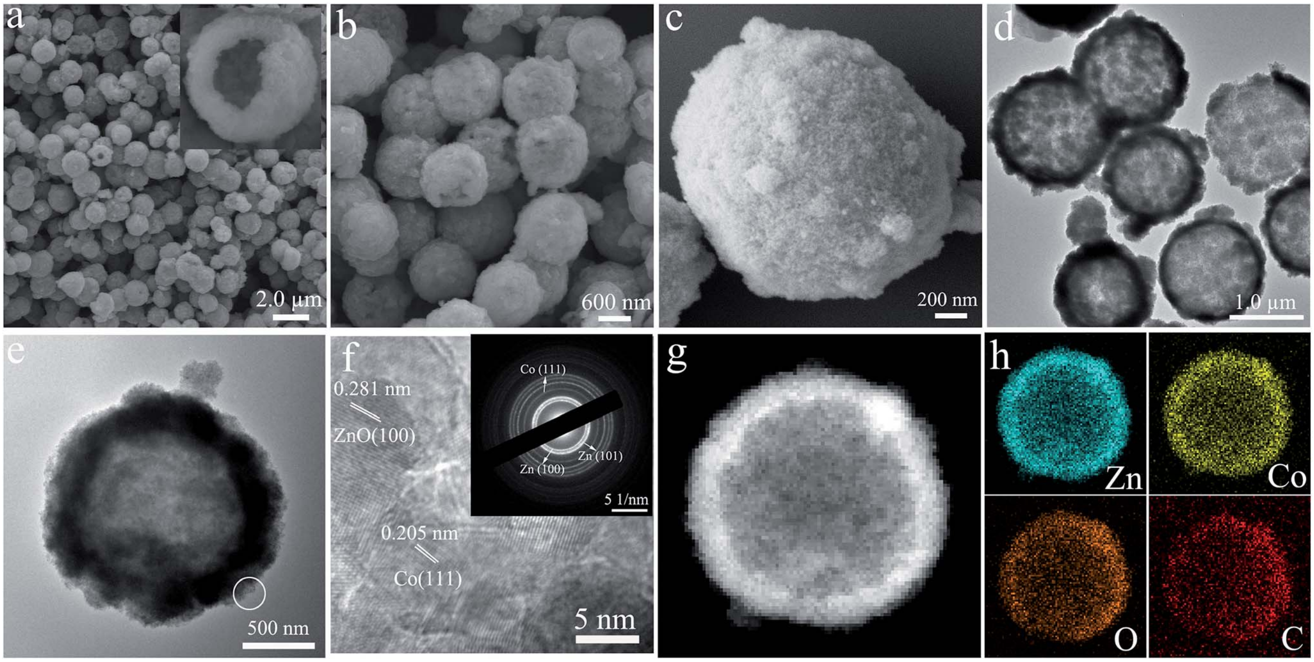

Fig. 4 The (a–c) SEM, (d and e) TEM, (f) HRTEM micrographs of ZnO–Co–C composites. The inset in (f) is the corresponding SAED pattern. (g) HAADF-STEM micrograph and (h) the element mappings of Zn, Co, O and C.

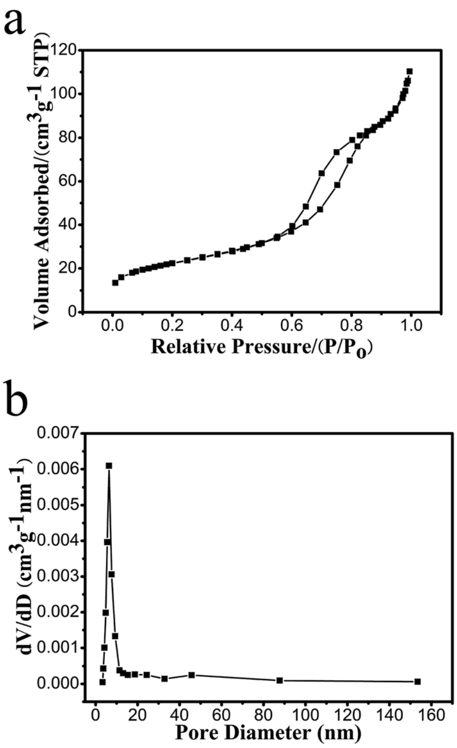

Fig. 5 (a) The BET surface area and (b) the corresponding pore diameter distribution of ZnO–Co–C.

precursor during the carbonation process. The mesopores provide good accessibility of the electrolyte into the electrode surface, facilitating the diffusion of Li^+ and the improvement of specific capacity.

The cyclic voltammogram (CV) profiles of ZnO–Co–C composites for the first three cycles are measured at 0.1 mV s^{-1} in the range 0.01–3 V and shown in Fig. 6a. There is a small reduction peak around 1.14 V in the first cathodic sweep, which may be due to the generation of SEI layers as a result of the decomposition of the electrolyte; this vanishes in the following cycles.[42] A broad and intense reduction peak centered at 0.27 V is visible, which is ascribed to the conversion reaction between ZnO and Li^+ to generate Zn and Li_2O as well as the subsequent alloying reaction between Zn and Li^+ to form Zn–Li alloys.[23,35] In the subsequent cycles, this cathodic peak moves to higher potential, which may be due to the changes in crystallinity and microstructures of active materials; this phenomenon is common for metal oxide-based anodes.[31,43] In the first anodic sweep, there are three small peaks between 0.1 and 0.8 V which are caused by the multi-step de-alloying reactions of Zn–Li alloys to regenerate the Zn nanocrystals.[34,44] The oxidation peak around 1.35 V originates from the decomposition of Li_2O and leads to the regeneration of ZnO.[45] A small amount of metallic Co that is electro-inactive to lithium ions only works as the conductive additive to strengthen the overall electronic conductivity of electrode materials, accounting for the absence of redox peaks caused by metallic Co in the CV profiles.[46] In the following CV scans, good superposition of redox peaks (in both position and shape) implies good reversibility of the electrochemical reactions.

The galvanostatic discharge–charge characterizations for the first two cycles of ZnO–Co–C are carried out at 200 mA g^{-1} between 0.01 and 3.0 V. As revealed in Fig. 6b, the ZnO–Co–C composite hollow microspheres demonstrate the discharge/charge capacities of 1390/975 mA h g^{-1} for the first cycle, relating to the initial coulombic efficiency of 70.1%. The low initial coulombic efficiency of metal oxide electrodes is caused by the irreversible formation of solid electrolyte interphase (SEI) layer on the surface of active particles as well as the incomplete decomposition of Li_2O, well known as an electrochemically irreversible material that results from the reduction of metal oxide anodes by lithium ions during the first discharge process.[47,48] As we know, the initial coulombic efficiency of electrode materials is one of the most momentous aspects to determine their practical application in lithium ion batteries. For comparison, the initial coulombic efficiencies of other ZnO-based anodes reported previously are summarized and shown in Fig. 6c.[34,48–52] For example, an initial coulombic efficiency of 56.6% was retained for an alumina-stabilized ZnO–graphene anode (ZnO–G-20).[34] ZnO quantum dot/graphene nanocomposites show an initial coulombic efficiency below 60.0%.[48] Peng's group reported that the Ag–C@ZnO–C@Ag–C hybrid hollow microspheres delivered an initial coulombic efficiency of about 65.4%.[49] It is worth pointing out that our ZnO–Co–C composites reveal one of the best initial coulombic efficiencies among other ZnO-based electrodes. It has been reported that transition metals, like Co, possess good electrocatalytic activity and are capable of activating or promoting the reversible decomposition of Li_2O and some SEI components, such as Li_2CoO_3, which may be beneficial for the improvement of the initial coulombic efficiency of ZnO–Co–C hybrids during the initial cycle.[26,29,53] Further studies are urgently needed to directly observe and corroborate this catalytic mechanism from the experimental point of view by means of the development of an *in situ* characterization technique. In the second cycle, the coulombic efficiency of ZnO–Co–C composite hollow microspheres increases to 91.8%, indicating the gradually enhanced electrochemical reaction reversibility.

The long-term cyclic properties are assessed at a current density of 200 mA g^{-1} within 0.01–3.0 V and the corresponding results are displayed in Fig. 6d. Distinctly, the reversible capacity of ZnO–Co–C decreases significantly in the first 40 cycles and then gradually shows a slight enhancement with cycle number. After 300 cycles, ZnO–Co–C delivers a decent discharge capacity of 794 mA h g^{-1} with a coulombic efficiency over 99.4%. For comparison, ZnO–C solid microspheres are also fabricated by annealing the zinc citrate solid microspheres with rough surfaces in an Ar atmosphere under the same conditions as those used for ZnO–Co–C composites, and the cycling performance of these ZnO–C solid microspheres is examined at 100 mA g^{-1} within 0.01–3.0 V. As shown in Fig. 6d, the reversible capacity of ZnO–C solid microspheres deteriorates rapidly with cycle number and only 233 mA h g^{-1} of discharge capacity can be retained after 100 cycles. Undoubtedly, ZnO–Co–C composite hollow microspheres deliver higher specific capacity and better

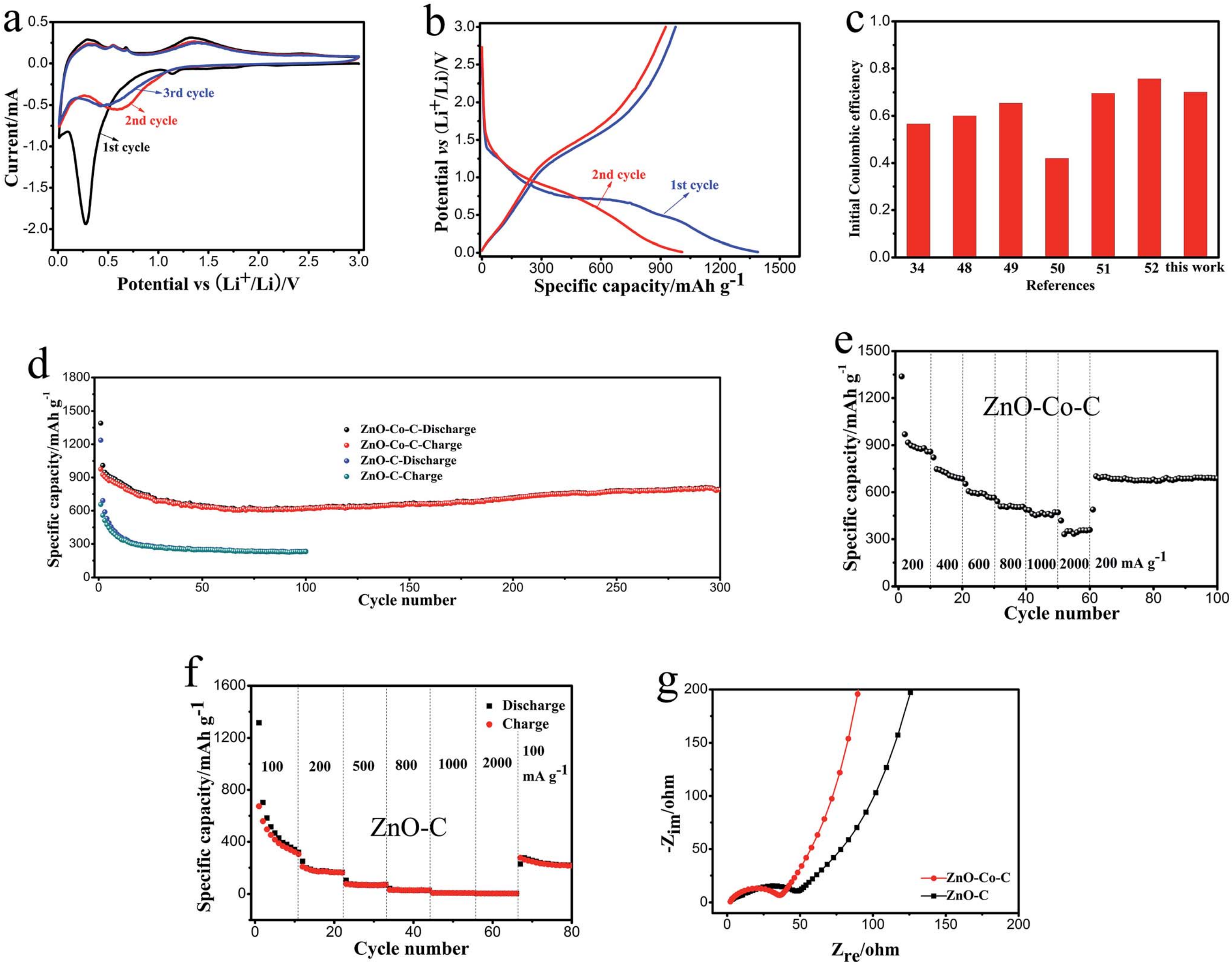

Fig. 6 (a) The CV profiles, (b) galvanostatic potential–capacity curves of ZnO–Co–C. (c) The comparison of initial coulombic efficiency of ZnO-based electrodes. (d) The cycling performances for ZnO–Co–C composites at 200 mA g^{-1} and ZnO–C solid microspheres at 100 mA g^{-1}. The rate performances at varied current density of (e) ZnO–Co–C hollow composites and (f) ZnO–C solid microspheres. (g) The electrochemical impedance spectra of ZnO–Co–C and ZnO–C composites.

cyclability than the ZnO–C counterparts. Table 1 shows the comparison of cycling performance between ZnO–Co–C composite hollow microspheres and other ZnO-based electrodes reported earlier. For instance, Co-modified ZnO coated with carbon prepared by Yang's group delivered a specific capacity of 725 mA h g^{-1} after cycling 50 times at 100 mA g^{-1}.[39] A reversible capacity of 653.7 mA h g^{-1} was obtained for a ZnO-M/PC electrode after cycling 100 times at 100 mA g^{-1}.[55]

Table 1 The comparison of cycling performance for various ZnO-based electrodes

Electrode materials	Morphology	Reversible capacity/mAh g^{-1}	Cycles	Ref.
ZnO–C	Yolk–shelled particles	520	150	7
ZnO–C	Nanocomposites	637	200	54
ZnO–Ag–C	Porous microspheres	729	200	23
C–Au@ZnO	Multipods	831	150	31
ZnO–graphene	Nano-hybrids	487	100	34
Co–ZnO@C	Cubic microparticles	725	50	39
ZnO–C	Nanoparticles	654	100	55
ZnO–Cu–C	Nanofibers	812	50	63
ZnO–$ZnFe_2O_4$	Sub-microcubes	837	200	56
ZnO–Co–C	Composite hollow microspheres	794	300	Our study

Hierarchical mesoporous bi-component-active ZnO/ZnFe_2O_4 sub-microcubes displayed a specific capacity of about 837 mA h g^{-1} after 200 cycles at 1000 mA g^{-1}.[56] Evidently, the fabricated ZnO–Co–C composites reveal a relatively high reversible capacity and good cyclability, which can be understood by considering the following two aspects. On one hand, the hollow architectures of ZnO–Co–C composites can provide an extra accommodating space for the drastic volume expansion of ZnO-active materials (Fig. 7a), helping to maintain the structural integrity and prevent pulverization of electrode.[7,11] Furthermore, the relatively large specific surface area of ZnO–Co–C hybrids endows more active sites to react with lithium ions, facilitating the enhancement of reversible capacity.[57] On the other hand, the conductive 3D carbon network derived from the *in situ* carbonation of carboxylate acid groups ($-COO^-$) in the zinc–cobalt citrate precursor is capable of effectively enhancing the electronic conductivity of ZnO active particles, benefitting the cycling performance of ZnO–Co–C composite anodes.[54,58–62] Furthermore, in order to clearly show the merits of the decoration of metallic Co, electrochemical impedance spectra measurements of ZnO–Co–C and ZnO–C composites were carried out, and the results are shown in Fig. 6g. A smaller diameter of the depressed semicircle in high frequency suggests a smaller charge transfer resistance and an enhanced electronic conductivity of ZnO–Co–C composites in comparison with the ZnO–C counterparts, which is beneficial for the improvement of lithium storage properties. Moreover, the modification of Co and C can prohibit the volume variation of ZnO to some extent, playing a vital role in acquiring a good cyclic lifespan.[39,64] In order to explicitly elucidate this behavior, after cycling 100 times, the electrode material is taken out and characterized by SEM. As illustrated in Fig. 7b, the hollow microspherical morphology (indicated by white arrows) of ZnO–Co–C composites is well preserved, evidencing their good structural stability.

The rate capability of electrode materials is another vital electrochemical parameter that must be considered for large-scale application in lithium ion batteries. As exhibited in Fig. 6e, the average specific capacity of ZnO–Co–C composite hollow microspheres decreases gradually from 937.2 to 724.6, 592.6, 509.1, 464.1 and finally 355.5 mA h g^{-1} with current density increasing from 200 to 400, 600, 800, 1000 and finally 2000 mA g^{-1}. One can observe that, even when cycled at a large current density of 2000 mA g^{-1}, a discharge capacity of 355.5 mA h g^{-1} is retained, which is comparable to the theoretical capacity of a commercial graphite anode. When the current density reduces back to 200 mA g^{-1}, our ZnO–Co–C composite hollow microspheres still show that outstanding cycling performance and a stable discharge capacity of 689 mA h g^{-1} can be achieved after a total of 100 cycles. By contrast, ZnO–C solid microspheres exhibit evident capacity deterioration as current density increases from 100 to 2000 mA g^{-1}, indicating an inferior rate capability (Fig. 6f). The greatly enhanced rate capability of ZnO–Co–C composites compared to ZnO–C counterparts is due to the doping of metallic Co, which can further strengthen the electronic conductivity of ZnO (Fig. 6g and 7a), giving rise to greatly enhanced electrochemical reaction kinetics. In addition, the nanoscale building blocks and the mesoporous feature of ZnO–Co–C composites are capable of shortening the diffusion distance of lithium ions and facilitating electrolyte transportation within the entire microsphere, respectively, which is helpful to enhance the rate capability.

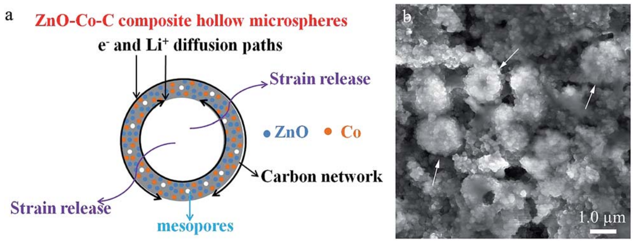

Fig. 7 (a) Schematic of the structural merits of ZnO–Co–C composite hollow microspheres. (b) SEM micrograph of ZnO–Co–C composite hollow microspheres after 100 cycles.

4. Conclusion

In conclusion, a facile approach has been put forward to synthesize ZnO–Co–C composite hollow microspheres, which consist of numerous well-dispersed ZnO and Co nanoparticles as well as a three-dimensional carbon network. When functioning as the active materials in lithium ion batteries, electrochemical investigations indicate that these ZnO–Co–C hybrids show relatively high reversible capacity, remarkable cyclability and exceptional rate performance. A greatly enhanced initial coulombic efficiency of 70.1% is achieved. After repetitive cycling for 300 times, ZnO–Co–C composite hollow microspheres deliver a decent discharge capacity of 794 mA h g^{-1}. The superior lithium storage properties of ZnO–Co–C composites result from their unique structural features, including the hollow construction, and doping of Co and C along with the nanoscale building blocks. This simple avenue should be employed to fabricate other metal oxides with metal or carbon modifications, which may hold bright prospects as advanced lithium ion battery anodes.

Acknowledgements

This study was supported by the National Natural Science Foundation of China (No. 51407034).

References

1 M. Armand and J. M. Tarascon, *Nature*, 2008, **451**, 652–657.
2 P. Meduri, E. Clark, E. Dayalan, G. U. Sumanasekera and M. K. Sunkara, *Energy Environ. Sci.*, 2011, **4**, 1695–1699.
3 J. M. Tarascon and M. Armand, *Nature*, 2001, **414**, 359–367.
4 B. N. Joshi, S. An, H. S. Jo, K. Y. Song, H. G. P. S. Hwang, S. S. Al-Deyab, W. Y. Yoon and S. S. Yoon, *ACS Appl. Mater. Interfaces*, 2016, **8**, 9446–9453.
5 M. V. Reddy, G. V. S. Rao and B. V. Chowdari, *Chem. Rev.*, 2013, **113**, 5364–5457.

6 J. Jiang, Y. Li, J. Liu, X. Huang, C. Yuan and X. W. Lou, *Adv. Mater.*, 2012, **24**, 5166–5180.
7 Q. Xie, X. Zhang, X. Wu, H. Wu, X. Liu, G. Yue, Y. Yang and D. L. Peng, *Electrochim. Acta*, 2014, **125**, 659–665.
8 X. Wang, Y. Fan, R. A. Susantyoko, Q. Xiao, L. Sun, D. He and Q. Zhang, *Nano Energy*, 2014, **5**, 91–96.
9 Z. Bai, Z. Ju, C. Guo, Y. Qian, B. Tang and S. Xiong, *Nanoscale*, 2014, **6**, 3268–3273.
10 J. S. Cho, Y. J. Hong and Y. C. Kang, *ACS Nano*, 2015, **9**, 4026–4035.
11 Z. Wang, L. Zhou and X. W. Lou, *Adv. Mater.*, 2012, **24**, 1903–1911.
12 J. Wang, N. Yang, H. Tang, Z. Dong, Q. Jin, M. Yang, D. Kisailus, H. Zhao, Z. Tang and D. Wang, *Angew. Chem.*, 2013, **125**, 6545–6548.
13 L. Hu, Y. Huang, F. Zhang and Q. Chen, *Nanoscale*, 2013, **5**, 4186–4190.
14 L. Shen, H. Song, G. Yang and C. Wang, *ACS Appl. Mater. Interfaces*, 2015, **7**, 11063–11068.
15 F. X. Ma, H. Hu, H. B. Wu, C. Y. Xu, Z. Xu, L. Zhen and X. W. Lou, *Adv. Mater.*, 2015, **27**, 4097–4101.
16 G. Zhang and X. W. Lou, *Adv. Mater.*, 2013, **25**, 976–979.
17 Y. Zhao, X. Li, L. Dong, B. Yan, H. Shan, D. Li and X. L. Sun, *Int. J. Hydrogen Energy*, 2015, **40**, 14338–14344.
18 Y. Wang, S. Wang, T. Zhao, Y. Chen, Z. Li, W. Wu and M. Wu, *Chem. Eng. J.*, 2016, **306**, 336–343.
19 W. Wei, W. Lv, M. B. Wu, F. Y. Su, Y. B. He, B. Li, F. Kang and Q. H. Yang, *Carbon*, 2013, **57**, 530–536.
20 Z. Li, G. Wu, S. Deng, S. Wang, Y. Wang, J. Zhou, S. Liu, W. Wu and M. Wu, *Chem. Eng. J.*, 2016, **283**, 1435–1442.
21 Y. Zhao, X. Li, B. Yan, D. Xiong, D. Li, S. Lawes and X. Sun, *Adv. Energy Mater.*, 2016, **6**, 1502175.
22 C. Yan, G. Chen, X. Zhou, J. Sun and C. Lv, *Adv. Funct. Mater.*, 2016, **26**, 1428–1436.
23 Q. Xie, Y. Ma, D. Zeng, X. Zhang, L. Wang, G. Yue and D. L. Peng, *ACS Appl. Mater. Interfaces*, 2014, **6**, 19895–19904.
24 Y. Zhao, X. Li, B. Yan, D. Li, S. Lawes and X. Sun, *J. Power Sources*, 2015, **274**, 869–884.
25 B. Luo and L. Zhi, *Energy Environ. Sci.*, 2015, **8**, 456–477.
26 L. Su, Z. Zhou and P. Shen, *J. Phys. Chem. C*, 2012, **116**, 23974–23980.
27 L. Zhang, P. Hu, X. Zhao, R. Tian, R. Zou and D. Xia, *J. Mater. Chem.*, 2011, **21**, 18279–18283.
28 L. Su, Z. Zhou and P. Shen, *Electrochim. Acta*, 2013, **87**, 180–185.
29 W. S. Kim, Y. Hwa, H. C. Kim, J. H. Choi, H. J. Sohn and S. H. Hong, *Nano Res.*, 2014, **7**, 1128–1136.
30 K. T. Park, F. Xia, S. W. Kim, S. B. Kim, T. Song, U. Paik and W. I. Park, *J. Phys. Chem. C*, 2013, **117**, 1037–1043.
31 B. Oschmann, M. N. Tahir, F. Mueller, D. Bresser, I. Lieberwirth, W. Tremel, S. Passerini and R. Zentel, *Macromol. Rapid Commun.*, 2015, **36**, 1075–1082.
32 Q. Xie, D. Zeng, Y. Ma, L. Lin, L. Wang and D. L. Peng, *Electrochim. Acta*, 2015, **169**, 283–290.
33 G. Z. Yang, H. W. Song, H. Cui, Y. C. Liu and C. X. Wang, *Nano Energy*, 2013, **2**, 579–585.
34 M. Yu, A. Wang, Y. Wang, C. Li and G. Shi, *Nanoscale*, 2014, **6**, 11419–11424.
35 G. Zhang, S. Hou, H. Zhang, W. Zeng, F. Yan, C. C. Li and H. Duan, *Adv. Mater.*, 2015, **27**, 2400–2405.
36 Q. Xie, J. Li, Q. Tian and R. Shi, *J. Mater. Chem.*, 2012, **22**, 13541–13547.
37 Q. Xie, Y. Ma, D. Zeng, L. Wang, G. Yue and D. L. Peng, *Sci. Rep.*, 2015, **5**, 8351.
38 J. Bartelmess, S. J. Quinn and S. Giordani, *Chem. Soc. Rev.*, 2015, **44**, 4672–4698.
39 H. Yue, Z. Shi, Q. Wang, Z. Cao, H. Dong, Y. Qiao, Y. Yin and S. Yang, *ACS Appl. Mater. Interfaces*, 2014, **6**, 17067–17074.
40 Q. Xie, Y. Ma, X. Zhang, H. Guo, A. Lu, L. Wang, G. Yue and D. L. Peng, *Electrochim. Acta*, 2014, **141**, 374–383.
41 A. Vu, Y. Qian and A. Stein, *Adv. Energy Mater.*, 2012, **2**, 1056–1085.
42 N. Li, S. X. Jin, Q. Y. Liao and C. X. Wang, *ACS Appl. Mater. Interfaces*, 2014, **6**, 20590–20596.
43 J. Xu, L. He, Y. Wang, C. Zhang and Y. Zhang, *Electrochim. Acta*, 2016, **191**, 417–425.
44 L. Qiao, X. Wang, L. Qiao, X. Sun, X. Li, Y. Zheng and D. He, *Nanoscale*, 2013, **5**, 3037–3042.
45 C. Xiao, S. Zhang, S. Wang, Y. Xing, R. Lin, X. Wei and W. Wang, *Electrochim. Acta*, 2016, **189**, 245–251.
46 N. Mahmood, C. Zhang, F. Liu, J. Zhu and Y. Hou, *ACS Nano*, 2013, **7**, 10307–10318.
47 Y. M. Kang, K. T. Kim, J. H. Kim, H. S. Kim, P. S. Lee, J. Y. Lee, H. K. Liu and S. X. Dou, *J. Power Sources*, 2004, **133**, 252–259.
48 X. Sun, C. Zhou, M. Xie, H. Sun, T. Hu, F. Lu, S. M. Scott, S. M. George and J. Lian, *J. Mater. Chem. A*, 2014, **2**, 7319–7326.
49 Q. Xie, Y. Ma, X. Wang, D. Zeng, L. Wang, L. Mai and D. L. Peng, *ACS Nano*, 2016, **10**, 1283–1291.
50 L. Liu, C. Zhao, H. Zhao, Q. Zhang and Y. Li, *Electrochim. Acta*, 2014, **135**, 224–231.
51 S. J. Yang, S. Nam, T. Kim, J. H. Im, H. Jung, J. H. Kang, S. Wi, B. Park and C. R. Park, *J. Am. Chem. Soc.*, 2013, **135**, 7394–7397.
52 F. Zou, X. Hu, Z. Li, L. Qie, C. Hu, R. Zeng, Y. Jiang and Y. Huang, *Adv. Mater.*, 2014, **26**, 6622–6628.
53 B. Lu, R. Hu, J. Liu, J. Liu, H. Wang and M. Zhu, *RSC Adv.*, 2016, **6**, 13384–13391.
54 P. Li, Y. Liu, J. Liu, Z. Li, G. Wu and M. Wu, *Chem. Eng. J.*, 2015, **271**, 173–179.
55 X. Shen, D. Mu, S. Chen, B. Wu and F. Wu, *ACS Appl. Mater. Interfaces*, 2013, **5**, 3118–3125.
56 L. Hou, L. Lian, L. Zhang, G. Pang, C. Yuan and X. Zhang, *Adv. Funct. Mater.*, 2015, **25**, 238–246.
57 X. Xie, C. Zhang, M.-B. Wu, Y. Tao, W. Lv and Q.-H. Yang, *Chem. Commun.*, 2013, **49**, 11092–11094.
58 G. Wu, Z. Li, W. Wu and M. Wu, *J. Alloys Compd.*, 2014, **615**, 582–587.
59 M. Wu, J. Liu, M. Tan, Z. Li, W. Wu, Y. Li, H. Wang, J. Zheng and J. Qiu, *RSC Adv.*, 2014, **4**, 25189–25194.

60 P. Li, J. Liu, Y. Liu, Y. Wang, Z. Li, W. Wu, Y. Wang, L. Yin, H. Xia, M. Wu, X. He and J. Qiu, *Electrochim. Acta*, 2015, **180**, 164–172.

61 F. Yang, P. Zhao, X. Hua, W. Luo, G. Cheng, W. Xing and S. Chen, *J. Mater. Chem. A*, 2016, **4**, 16057–16063.

62 X. Peng, J. Qu, S. Tian, Y. Ding, X. Hai, B. Jiang, M. Wu and J. Qiu, *RSC Adv.*, 2016, **6**, 104549–104555.

63 X. Shen, D. Mu, S. Chen, R. Huang and F. Wu, *J. Mater. Chem. A*, 2014, **2**, 4309–4315.

64 Y. J. Mai, X. H. Xia, R. Chen, C. D. Gu, X. L. Wang and J. P. Tu, *Electrochim. Acta*, 2012, **67**, 73–78.